ORGANOMETALLICS

ARTICLE

pubs.acs.org/Organometallics

How Racemic Secondary Alkyl Electrophiles Proceed to Enantioselective Products in Negishi Cross-Coupling Reactions

Xufeng Lin,*[,†,‡] Jian Sun,[‡] Yanyan Xi,[†] and Delian Lin[†]

[†]State Key Laboratory of Heavy Oil Processing, College of Chemistry & Chemical Engineering, China University of Petroleum (East China), Qingdao, 266555, People's Republic of China

[‡]Department of Chemistry, The University of Hong Kong, Pokfulam Road, Hong Kong, People's Republic of China

Supporting Information

ABSTRACT: Two mechanisms, namely, the Ni(0)−Ni(II) and Ni(I)−Ni(III) mechanisms, for nickel-bis(oxazolinyl)pyridine complex catalyzed Negishi cross-coupling reaction were investigated with density functional calculations. The Ni(I)−Ni(III) mechanism, containing sequential steps of transmetalation−oxidative addition−reductive elimination, is more favorable than the Ni(0)−Ni(II) mechanism, based on the energetic span model. The enantioselectivity of the coupled product from a racemic secondary alkyl electrophile was calculated by the relative reaction rate (r_S/r_R) of the reductive elimination step that forms the coupled product in the *S*-enantiomer over that leading to the *R*-enantiomer. The r_S/r_R can be calculated from the relative free energy of the transition states for these two reductive elimination pathways in the Ni(I)−Ni(III) mechanism. The calculated enantioselectivity for the model reaction is consistent with the experimental report. The influence of the asymmetric steric hindrance of the catalyst ligand on the reductive elimination step is also discussed.

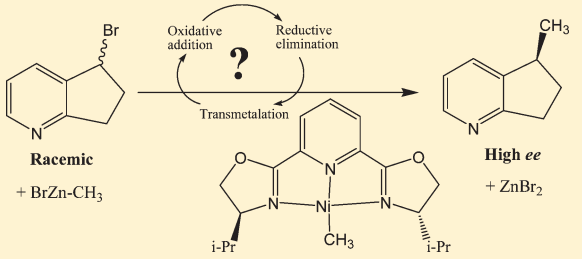

INTRODUCTION

Ni or Pd complex catalyzed cross-coupling reactions between organo-electrophiles (typically organohalides) and organo-nucleophiles (typically alkylmetal halides, e.g., EtZnI) are widely used methods for building desired molecules by C−C bond formation.[1,2] However, the formation of a C(sp^3)−C(sp^3) bond with an alkyl electrophile, especially with a secondary alkyl electrophile, is much more difficult than a C−C bond formation with an aryl or vinyl eletrophile. In recent years obvious progress has been made in developing cross-coupling reactions of secondary alkyl electrophiles by Fu and co-workers.[3−5] They reported nickel-catalyzed reactions using the bis(oxazolinyl)pyridine ligands that successfully achieved Negishi coupling of unactivated secondary alkyl bromides.[3] The variety of catalyst ligand scaffolds and the steric properties of the alkyl electrophiles may lead to different product selectivity. The first example of catalytic asymmetric cross-coupling of secondary electrophiles was achieved by exploiting the C_2 symmetry of the catalyst ligand, when employing α-bromoamides as substrates.[4] In ref 4a they established that a family of reaction partners, racemic secondary benzylic halides, can be coupled with organozinc reagents in very good enantiomeric excess (ee), as expressed in reaction A in Scheme 1 (see the notations of the catalyst ligand as well). Upon investigation of a variety of conditions and substituents R and R^2, they determined that Negishi reactions of 1-bromoindanes proceed in yields ranging from 39% to 89% and the ee value ranging from 90% to 98%. (*R*)-(*i*-Pr)-Pybox was also used for the synthesis of (*R*)-1-methyl-3-oxo-indene, with an ee value of 92%.[4b] Although there was no report of mechanistic studies to account for the stereoconvergence, the involvement of a radical in these systems has been suggested.[4b,c]

Due to the great significance of asymmetric catalysis, the conversion of racemic alkyl halides to high ee value products greatly interests us. The explanation/prediction of ee values calls for deep insight into the reaction mechiansm for Ni complex catalyzed Negishi cross-coupling reactions. Although the textbook mechanism for cross-coupling reactions containing sequential steps of oxidative addition−transmetalation−reductive elimination has been established for more than three decades,[1] several researchers[6−9] have pointed out that this mechanism is not feasible for C(sp^3)−C(sp^3) cross-coupling reactions. Actually in the expanding numbers of works on cross-coupling reactions, it can be found in the literature that the textbook mechanism may not be feasible (or need modification) even for some non-C(sp^3)−C(sp^3) cross-coupling reactions.[2d,10,11] The reaction mechanism for C(sp^3)−C(sp^3) cross-coupling is still elusive in the literature. For nickel-terpyridine complex catalyzed Negishi alkyl−alkyl cross-coupling reactions, it has been experimentally[8] and theoretically[9] suggested that the sequential steps of oxidative addition−reductive−transmetalation working with the Ni(I)−Ni(III) cycles may be plausible.

Similar to terpyridines, Pybox and its derivatives are another family of trinitrogen ligands. In this work we explored the

Received: December 28, 2010
Published: June 01, 2011

Scheme 1. Real[4a] (A) and Model (B) Negishi Cross-Coupling Reactions Studied in this Paper[a]

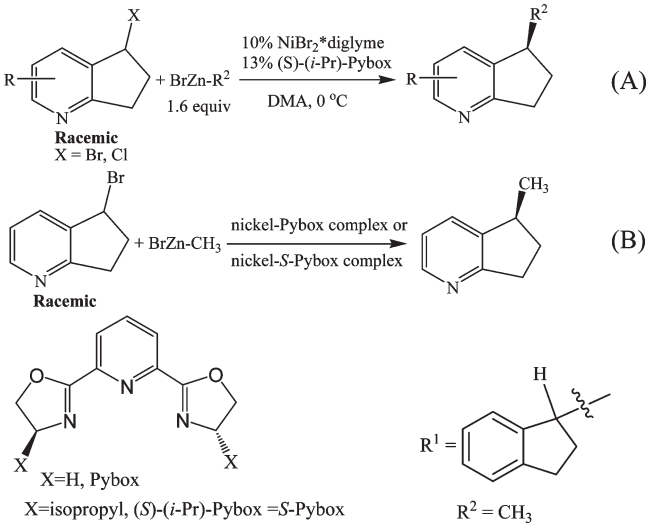

[a] R^1 and R^2 denote α-indenyl and methyl as indicated, respectively. Two catalyst ligands, namely, Pybox and *S*-Pybox, as indicated, were examined in this paper.

potential energy surfaces (PES) of two mechanisms for reaction B to model reaction A (Scheme 1) by density functional theory (DFT) calculations. The Ni(I)−Ni(III) mechanism instead of the Ni(0)−Ni(II) one (textbook mechanism applying to reaction B) is feasible based on the energetic span model. Then, based on the Ni(I)−Ni(III) catalytic cycle, the relative rates of formation of products (r_S/r_R) in both *S*- and *R*-enantiomers were calculated. The calculated r_S/r_R for reaction B is consistent with the experimental report by Fu and co-workers.[4a] We believe that this work provides deep insight into the mechanism for metal-catalyzed cross-coupling with C(sp^3)−C(sp^3) bond formation reactions, especially for the enantioselectivity-determining step(s). More importantly, the method for calculation/prediction of the enantioselectivity for this type of reaction will help synthetic chemists design/select their catalyst ligands and the structure of reactants for asymmetric synthesis.

COMPUTATIONAL METHODS

Density functional calculations were performed using the hybrid B3LYP[12] exchange and correlation functionals in order to explore the potential energy surfaces of the model Ni-catalyzed Negishi alkyl−alkyl cross-coupling reactions. The 6-31G* basis set was used for all C, H, O, N, Ni, Zn, and Br atoms. Five component d functions were employed in the calculations. The B3LYP/6-31G* level of theory is appropriate to calculate the PES of Ni-trinitrogen ligand complex catalyzed cross-coupling reactions, as reported in the previous study.[9]

The PES for the reactions of interest were explored by optimizing geometries in the energy minima for the reactants, the intermediates, and the products, and the first-order saddle points for transition states using the Gaussian 03 program suite (employing C.02 version).[13] Vibrational analyses were performed to confirm energy minima and first-order saddle points as well as to obtain the zero-point-corrected energies (ZPE) and free energies (at 273.15 K) of the optimized geometries. As reaction A was carried out in dimethylacetamide (DMA) as solvent, bulk solvation effects were examined with the polarized continuum model (PCM)[14] utilizing DMSO to model DMA.[15] Intrinsic reaction coordinate (IRC) computations were done to confirm the transition states connecting the appropriate reactants and products.[16]

RESULTS AND DISCUSSION

To save computational resources, Pybox instead of *S*-Pybox (see Scheme 1 for the notations) was used to examine the potential energy surfaces of the Ni(0)−Ni(II) and Ni(I)−Ni(III) mechanisms in the first two subsections (subsections A and B).

(A) Ni(0)−Ni(II) Mechanism. The textbook[1] Ni(0)−Ni(II) mechanism for reaction B contains the following three steps:

$$\text{Oxidative addition}: \quad \text{Ni(Pybox)} + \text{Br-R}^1 \rightarrow \text{Br-Ni(Pybox)-R}^1 \tag{1}$$

$$\text{Transmetalation}: \quad \text{Br-Ni(Pybox)-R}^1 + \text{CH}_3\text{ZnBr} \rightarrow \text{CH}_3\text{-Ni(Pybox)-R}^1 + \text{ZnBr}_2 \tag{2}$$

$$\text{Reductive elimination}: \quad \text{CH}_3\text{-Ni(Pybox)-R}^1 \rightarrow \text{Ni(Pybox)} + \text{R}^1\text{-CH}_3 \tag{3}$$

Figure 1 presents the optimized geometries of species involved in eqs 1−3, and Figure 2 depicts the free energy profiles of these three steps. For the transmetalation step (eq 2), a reactant complex (denoted as **RC2**) and a product complex (denoted as **PC2**) were found, and a transition state (**TS2**) containing a four-membered-ring Br···Ni···C···Zn moiety can be identified. For the reductive elimination step (eq 3) starting from R^1-Ni(Pybox)-CH_3, a three-membered-ring Ni···C···C moiety can be seen in the transition state (**TS3**) structure. As proposed by Kozuch and co-workers,[17] the energetic span (δE) of a catalytic cycle determines if it is favorable or not. The lower δE, the more favorable the catalytic cycle is. The δE can be calculated from the energy difference between the turnover frequency determining transition state (TDTS) and the turnover frequency determining intermediate (TDI). Although the transition-state structure for the oxidative addition step (eq 1) was not examined, Figure 2 provides a lower limit of δE for the Ni(0)−Ni(II) catalytic cycle. If the free energy of the transition state (**TS1**) for eq 1 is not high enough to be a TDTS, then the TDI is the **RC2** formed from the R^1-Ni(Pybox)-Br and CH_3ZnBr in the transmetalation step, and the TDTS is the transition state of the reductive elimination step (**TS3** in eq 3). The energetic span calculated from the free energy of these two structures is 53.7 kcal/mol. If the free energy of **TS1** is high enough to be a TDTS, the real energetic span will be larger than 53.7 kcal/mol. The lower limit of δE for the Ni(0)−Ni(II) catalytic cycle will be compared to that for the Ni(I)−Ni(III) catalytic cycle, reported later, and conclusions will be drawn then.

(B) Ni(I)−Ni(III) Mechanism. The catalytic cycle working with the Ni(I)−Ni(III) mechanism for reaction B, similar to that reported in our previous work,[9] can be written as

$$\text{Ni(Pybox)-CH}_3 + \text{R}^1\text{-Br} \rightarrow \text{Ni(Pybox)-Br} + \text{R}^1\text{-CH}_3 \tag{4}$$

$$\text{Ni(Pybox)-Br} + \text{CH}_3\text{ZnBr} \rightarrow \text{Ni(Pybox)-CH}_3 + \text{ZnBr}_2 \tag{5}$$

Equation 4 is the combination of the following three steps:

$$\text{Ni(Pybox)-CH}_3 + \text{R}^1\text{-Br} \rightarrow \text{Br-Ni(Pybox)-CH}_3 + \text{R}^1\cdot \tag{6}$$

dx.doi.org/10.1021/om1012049 |*Organometallics* 2011, 30, 3284–3292

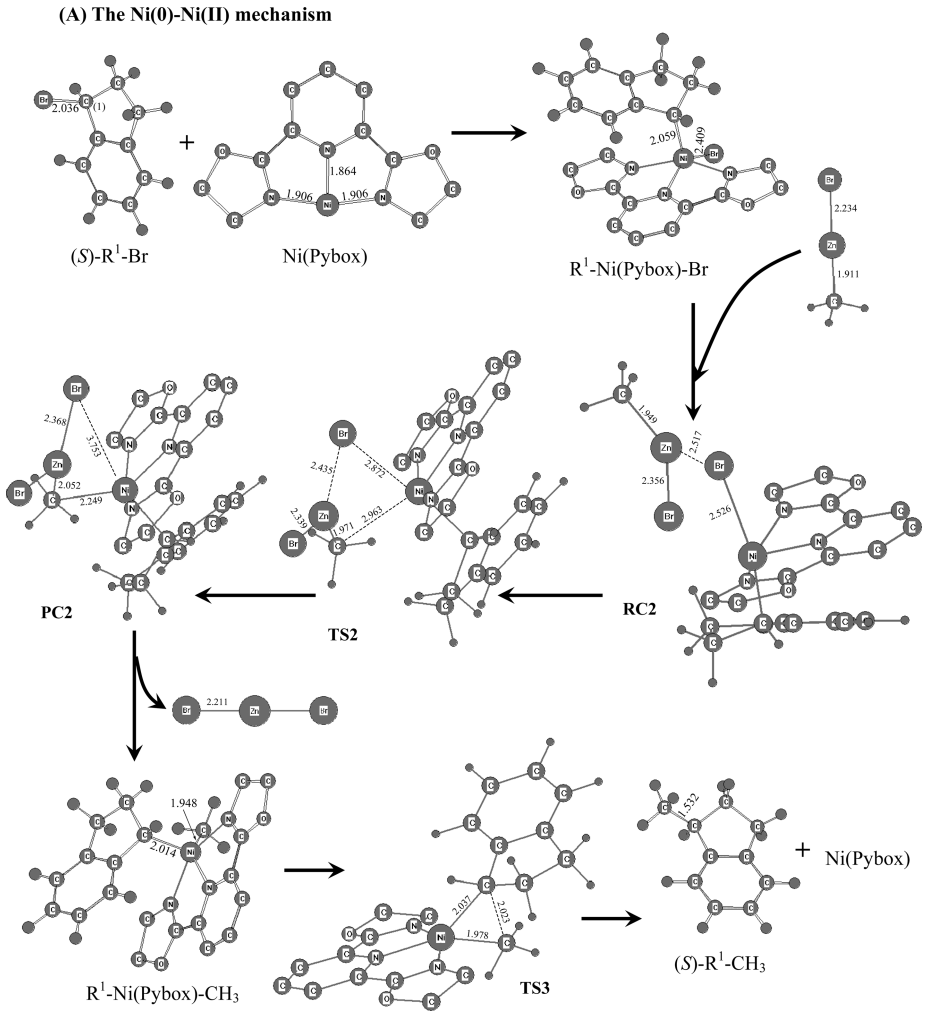

Figure 1. Optimized geometries at B3LYP/6-31G* level of theory for the species involved in eqs 1 and 2. Hydrogen atoms on Pybox are deleted for clarity in this and the following figures. Key bond lengths are indicated (in Å).

$$\text{Br-Ni(Pybox)-CH}_3 + \text{R}^1\cdot \rightarrow \text{CH}_3\text{-NiBr(Pybox)-R}^1 \quad (7)$$

$$\text{CH}_3\text{-NiBr(Pybox)-R}^1 \rightarrow \text{Ni(Pybox)-Br} + \text{R}^1\text{-CH}_3 \quad (8)$$

Equation 6 is the Br transfer step, eq 7 the R^1 radical attack step,[18,19] and eq 8 the reductive elimination step that results in the coupled product. The combination of eqs 6 and 7 can be considered as the oxidative addition step. The overall reaction of eqs 4 and 5 can be written as

$$\text{R}^1\text{-Br} + \text{CH}_3\text{ZnBr} \rightarrow \text{R}^1\text{-CH}_3 + \text{ZnBr}_2\,[\text{Ni(Pybox)-Br as catalyst}] \quad (9)$$

(a) eq 4: Ni(Pybox)-CH_3 in Reaction with Alkyl Bromide. Figure 3 presents the optimized geometries of the two Ni(I) species involved in eq 4. As the catalyst ligand of Pybox has a C_{2v} symmetry and (*S*)-R^1-Br (see Figure 1) and (*R*)-R^1-Br are the mirror images of each other, all the reactants, intermediates, transition states, and products of eq 4 in *S*-enantiomer form are all the mirror images of their corresponding *R*-enantiomer. The free energy profiles of eq 4 with the *S*-enantiomer form should be the same as those with *R*-enantiomer form (*vide infra*). A suffix of

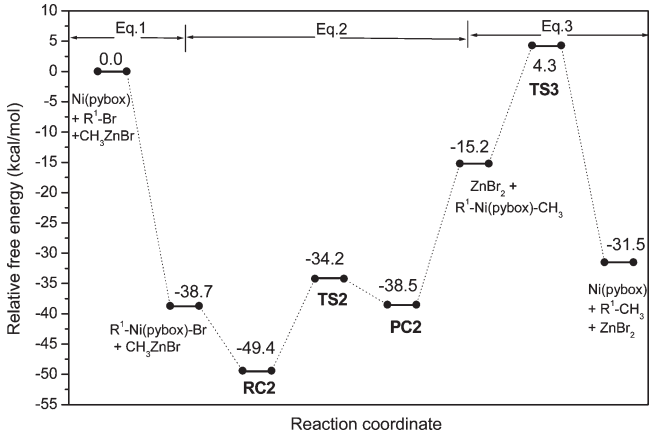

Figure 2. Free energy profile of the Ni(0)−Ni(II) mechanism.

"-*S*" was used for all the transition states and Ni(III) intermediates in the pathways that lead to the coupled product R^1-CH_3 in the *S*-enantiomer form, and here the results of eq 4 are presented only for the *S*-enantiomer production first.

dx.doi.org/10.1021/om1012049 |*Organometallics* 2011, 30, 3284–3292

Figure 4 presents all the geometries of the transition states, intermediates, and products involved in eqs 6−8. The transition state of the Br transfer step (eq 6), **TS6**-*S*, occurs at the Br···$C^{(1)}$ distance of 2.613 Å and the Br···Ni distance of 2.557 Å. The $C^{(1)}$, Br, and Ni atoms are roughly in a straight line. The products proceeding through **TS6**-*S* are a R^1 radical and the Ni(II) species [Br-Ni(Pybox)-CH_3], in which the Br−Ni bond length is 2.498 Å. Br-Ni(Pybox)-CH_3 also has a square-based pyramidal ML_5 structure, as in the case of I-Ni(tpy)-CH_3 in the previous work.[9] R^1 radical attack onto the Ni(II) species occurs at the other side of the Pybox plane with respect to the Br transfer step. The transition state of this step (**TS7**-*S* in Figure 4) occurs at the $C^{(1)}$···Ni distance of 2.852 Å in the reaction coordinate in terms of the $C^{(1)}$−Ni bond formation. The Ni(III)-*S* intermediate [CH_3-Ni(Pybox)Br-R^1] proceeding by **TS7**-*S* has a $C^{(1)}$−Ni bond length of 2.015 Å. The transition-state structure (**TS8**-*S*) of the reductive elimination step has a trigonal $C^{(1)}$−Ni−$C^{(2)}$ geometry with $C^{(1)}$−Ni, Ni−$C^{(2)}$, and $C^{(1)}$···$C^{(2)}$ distances of 2.150, 2.097, and 2.130 Å, respectively. The products proceeding by **TS8**-*S* consist of the coupled product R^1-CH_3 as the *S*-enantiomer, as well as another Ni(I) species, Ni(Pybox)-Br.

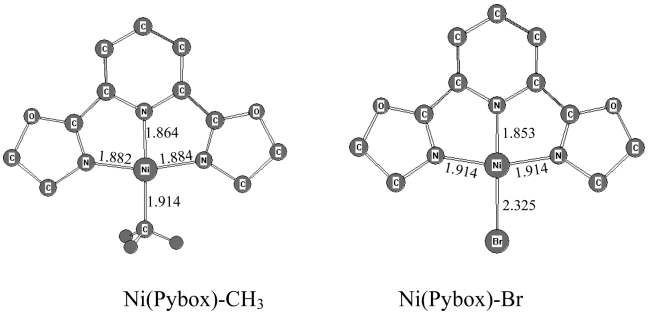

Figure 3. Optimized geometries of the two Ni(I) species involved in eq 4. Key bond lengths are indicated (in Å).

The free energy profiles of these three steps are presented in Figure 5. The Br transfer step (eq 6) has a free energy of activation of 14.2 kcal/mol and is slightly endothermic by 2.3 kcal/mol. The R^1 radical attack step (eq 7) has a free energy of activation of 14.4 kcal/mol and is slightly exothermic by 1.5 kcal/mol. So, the overall oxidation addition step (eqs 6 and 7) has two mildly large free energies of activation, and the free energy change is very small. The reductive elimination step (eq 8) needs a higher free energy of activation (20.3 kcal/mol) than the preceding two steps and is highly exothermic by a free energy decrease of 45.2 kcal/mol. The large exothermicity of eq 8 makes the overall reaction of eq 4 exothermic by 44.4 kcal/mol. These data indicate that, for sequential steps of Br transfer, radical attack, and reductive elimination, the former two steps are in fast equilibrium, and the reductive elimination step is irreversible and rate-determining in the process of Ni(Pybox)-CH_3 reacting with R^1-Br. This is dramatically different from the case of Ni(tpy)-CH_3 reacting with propyl/isopropyl iodide, in which the iodine atom transfer step is rate-determining.[9]

(b) eq 5: Ni(Pybox)-Br Transmetalating with CH_3ZnBr. For Ni(Pybox)-Br transmetalating with CH_3ZnBr to afford

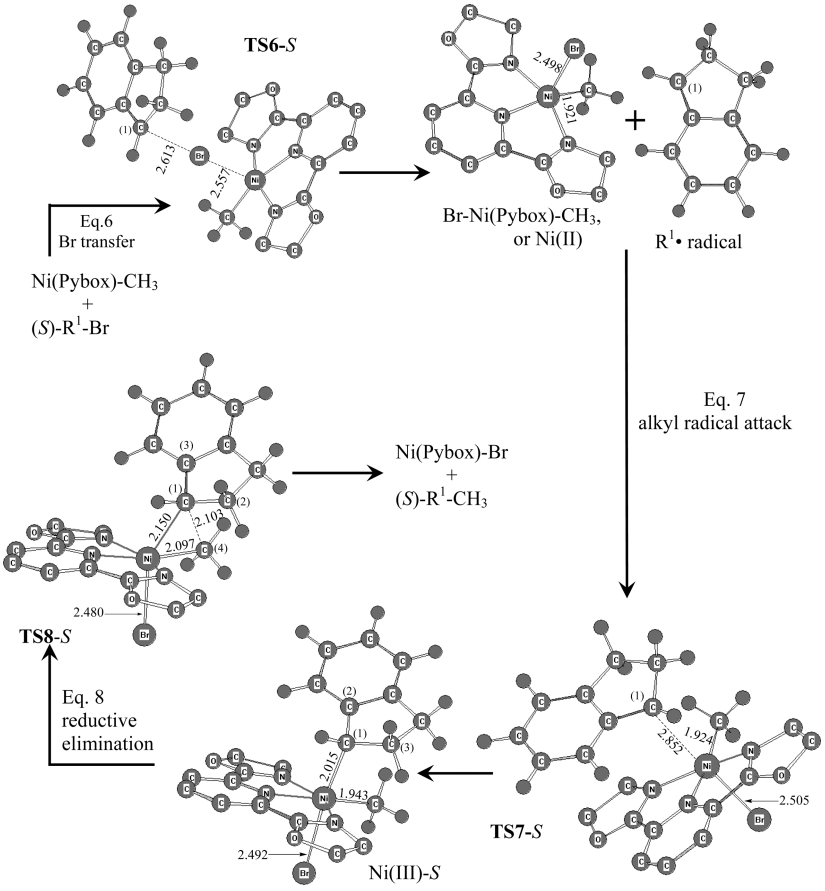

Figure 4. Optimized geometries of the transition states and intermediates in eqs 6−8 (or eq 4). Key bond lengths are indicated (in Å).

dx.doi.org/10.1021/om1012049 |*Organometallics* 2011, 30, 3284–3292

Ni(Pybox)-CH_3, a reactant complex (denoted as **RC5**) and a product complex (**PC5**), which are more stable than the separated products, were found. A four-membered-ring transition-state structure similar to the one for Ni(bipyridine)-I transmetalating with CH_3ZnI was reported by Cárdenas and co-workers.[10b] As the product of this transmetalation step is the reactant of the bromine transfer step (eq 6), the relative energy of the product in eq 5 is set to 0 kcal/mol. Therefore, if the free energy profiles for eqs 5−8 (in Figure 7 and Figure 5) are put together, one may see that the TDI for the Ni(I)−Ni(III) catalytic cycle is **RC5** in the transmetalation step (eq 5), and the TDTS is **TS8**-*S* in the reductive elimination step (eq 8). This situation is quite similar to the Ni(0)−Ni(II) cycle. However, the energetic span for the Ni(I)−Ni(III) cycle is 42.8 kcal/mol, which is significantly lower than the one (with the lower limit of 53.7 kcal/mol) for the Ni(0)−Ni(III) cycle (see subsection A). Therefore, the Ni(0)−Ni(II) mechanism is discarded in this paper in the following part for enantioselectivity calculation.

(c) No Enantioselectivity of the Coupled Product in the Case of C_{2v} Pybox Used As Ligand. As is mentioned above, all the reactants, intermediates, transition states, and products of eq 4 in *S*-enantiomer form are all chirally symmetric to those corresponding to the *R*-enantiomer. Since one of the main points in this paper is to show how the enantioselecitive product is produced in the presence of the C_2 *S*-Pybox ligand, it is necessary to verify that the C_{2v} symmetric ligand of Pybox does not lead to any enantioselectivity. In this work the transition states, intermediates, and the products involved in eq 4 that lead to (*R*)-R^1-CH_3 were also examined structurally and energetically. These geometries are, not surprisingly, the mirror images of the corresponding ones presented in Figure 4 (therefore, not presented in this paper), and the free energy profile is the same (the difference is no larger than 0.03 kcal/mol) as the one presented in Figure 5. Thus, for the Pybox ligand without a substitution group, the rates of all the steps producing the coupled product in the *R*-enantiomer are the same as those producing the *S*-enantiomer, which leads to no enantioselectivity for the cross-coupling reactions. On the other hand, computation of the pathways for producing the *R*-enantiomer with the C_{2v} ligand shows the computational error contributes little (<0.03 kcal/mol) to the difference of energy profiles for both enantiomers when the ligand is replaced with a C_2 ligand (*vide infra*).

(C) Ni(I)−Ni(III) Mechanism in the Case of C_2 Symmetric *S*-Pybox Used As Catalyst Ligand. *(a) Structural and Energetic Characterization of eqs 7 and 8 with the S-Pybox Ligand.* In the above sections it has been demonstrated that the textbook mechanism of sequential steps of oxidative elimination, transmetalation,

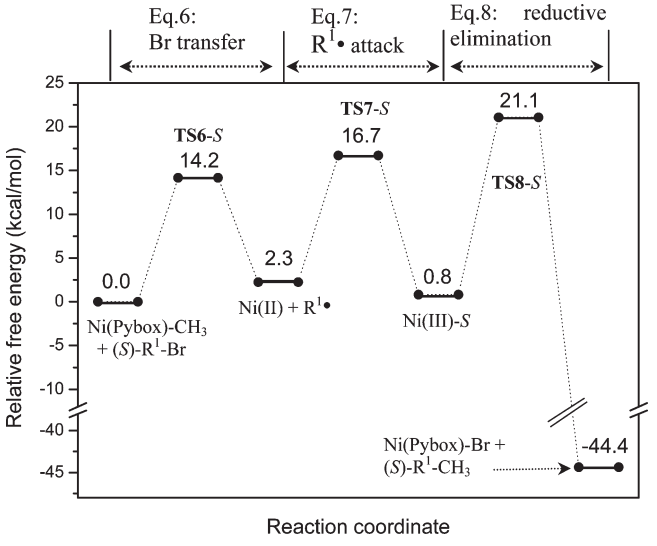

Figure 5. Free energy profile for the reaction between Ni(Pybox)-CH_3 and R^1-Br (eq 4 or eqs 6−8).

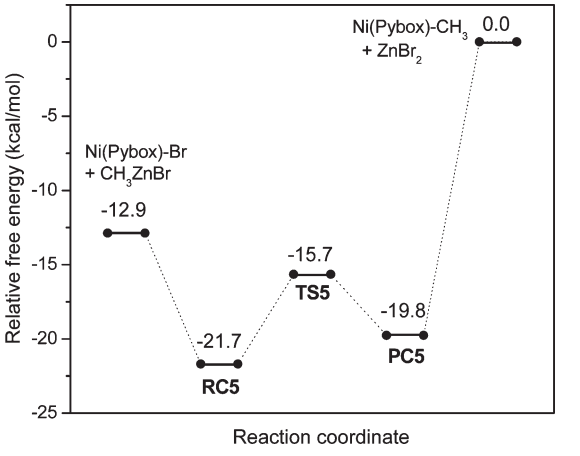

Figure 7. Relative free energy profile for the transmetalation step (eq 5) in the Ni(I)−Ni(III) mechanism.

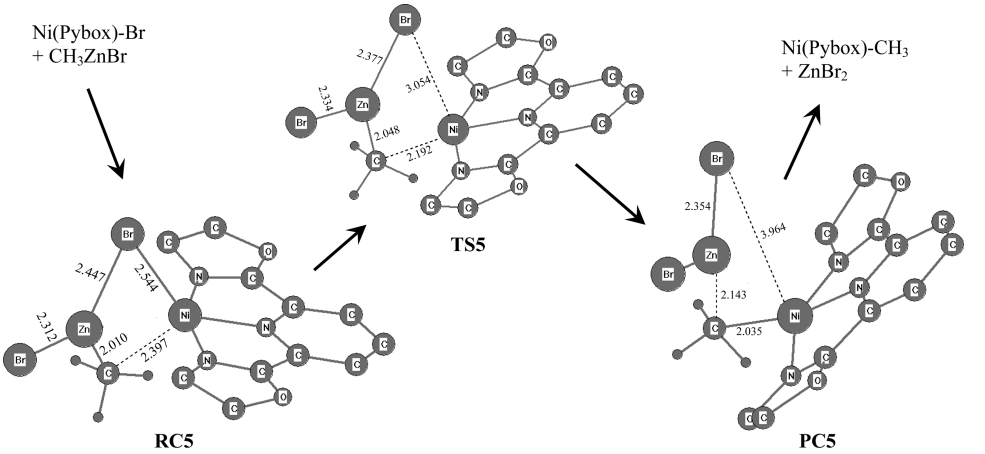

Figure 6. Optimized geometries of the species involved in eq 5. Key bond lengths are indicated (in Å).

and reductive elimination working with the Ni(0)−Ni(II) couple is not feasible thermodynamically, while the mechanism containing sequential steps of oxidative addition, reductive elimination, and transmetalation working with the Ni(I)−Ni(III) couple is feasible. The Ni(I) species [Ni(Pybox)-CH_3] acts as a catalyst for reaction B. The oxidative addition of aryl iodide occurring at a Ni(I)-binitrogen ligand complex was also proposed by Phaple et al.[10] Since only eqs 7 and 8 account for the formation of a new bond in the $C^{(1)}$ site in the R^1 moiety, only these two steps were examined in this work as presented hereafter.

If the catalyst ligand has a lower symmetry than Pybox, such as (*S*)-isopropyl-Pybox (*S*-Pybox) or (*R*)-isopropyl-Pybox, the structures of **TS7**-*S*, Ni(III)-*S*, and **TS8**-*S* will no longer be chirally symmetric with those of **TS7**-*R*, Ni(III)-*R*, and **TS8**-*R*, due to the presence of asymmetric steric hindrance. Thus, eqs 7 and 8 for the C_{2v} Pybox ligand should be replaced with the following four equations when the C_2 *S*-Pybox ligand is used:

$$\text{Br-Ni}(S\text{-Pybox})\text{-CH}_3 + \text{R}^1\cdot \rightarrow \text{CH}_3\text{-NiBr(Pybox)-R}^1 \ [S\text{-enantiomer}, S\text{-Ni(III)-}S] \quad \text{(S-7-S)}$$

$$\text{Br-Ni}(S\text{-Pybox})\text{-CH}_3 + \text{R}^1\cdot \rightarrow \text{CH}_3\text{-NiBr(Pybox)-R}^1 \ [R\text{-enantiomer}, S\text{-Ni(III)-}R] \quad \text{(S-7-R)}$$

$$\text{CH}_3\text{-NiBr}(S\text{-Pybox})\text{-R}^1 \ (S\text{-enantiomer}) \rightarrow \text{Ni(Pybox)-Br} + (S)\text{-R}^1\text{-CH}_3 \quad \text{(S-8-S)}$$

$$\text{CH}_3\text{-NiBr}(S\text{-Pybox})\text{-R}^1 \ (R\text{-enantiomer}) \rightarrow \text{Ni(Pybox)-Br} + (R)\text{-R}^1\text{-CH}_3 \quad \text{(S-8-R)}$$

A prefix of "*S*-" was used in the notations of the above four equations and in all the structures involved in these equations for indicating the ligand used here is *S*-Pybox. A suffix of "-*S*" or "-*R*" was used to represent the structures or equations that lead to the coupled product as an *S*- or *R*-enantiomer. For example, *S*-**TS8**-*R* denotes the transition state of eq *S*-8-*R*, the $C^{(1)}$ atom of which is in the *R*-conformation.

Figure 8 shows the optimized geometries of Br-Ni(*S*-Pybox)-CH_3 [*S*-Ni(II)] and the R^1 radical, as the reactants. The R^1 radical attacks the Ni atom in *S*-Ni(II) (eqs *S*-7-*S* and *S*-7-*R*) on the other side of the Pybox plane with respect to the Br atom. The Ni atom in *S*-Ni(II) attacking the $C^{(1)}$ atom in the R^1 radical at the Z^+ side (defined in Figure 8) matches the transition state *S*-**TS7**-*S* (see Figure 9) at the Ni···$C^{(1)}$ distance of 2.897 Å. In contrast, when the R^1 radical attack occurs at its Z^- side, the transition state (*S*-**TS7**-*R* in Figure 10) occurs at the Ni···$C^{(1)}$ distance of 3.090 Å. *S*-**TS7**-*R* is not the mirror image of *S*-**TS7**-*S*, and *S*-**TS7**-*R* comes earlier than *S*-**TS7**-*S* along the reaction coordinate in terms of the Ni−$C^{(1)}$ bond formation process.

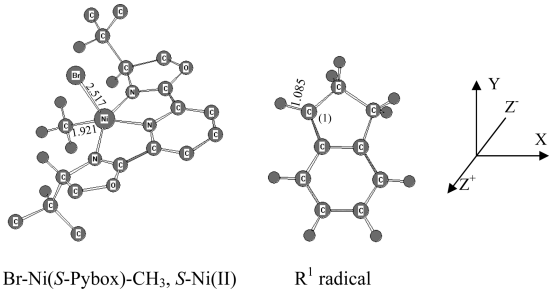

Figure 8. Optimized geometries of the reactant for the radical attack step (eqs *S*-7-*S* and *S*-7-*R*) in the Ni(*S*-Pybox)-CH_3-catalyzed cross-coupling reaction. For a better description of the two sides of the R^1 radical when it goes to the Ni atom (since they lead to different enantiomers in the coupled product), Z^+ and Z^- directions were defined by putting the benzene ring in the R^1 radical on the *XY* plane of a 3D Cartesian coordinate system as indicated. R^1 radical is symmetric with the *XY* plane.

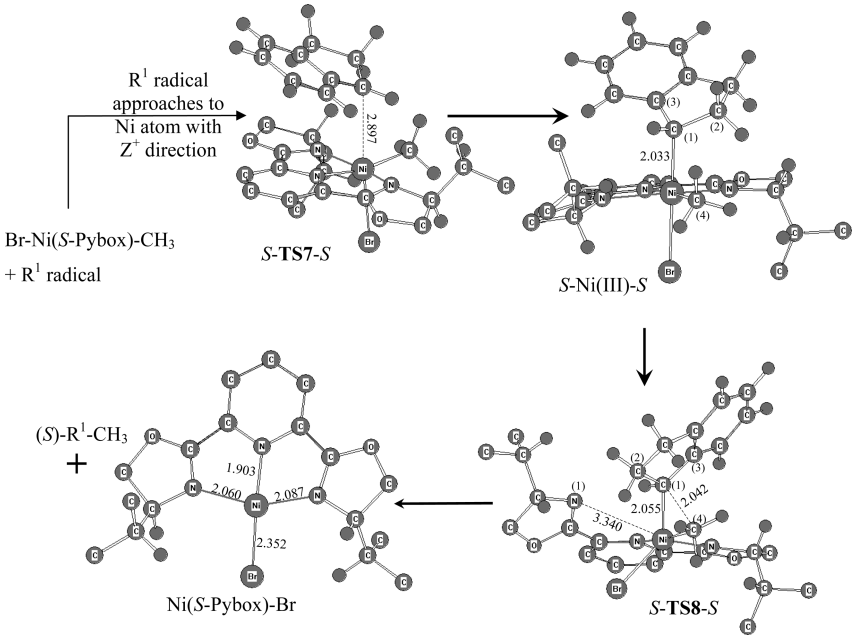

Figure 9. Optimized geometries for the intermediates, the transition states, and the products in the reaction that forms a cross-coupled product in *S*-enantiomer form with the ligand *S*-Pybox.

dx.doi.org/10.1021/om1012049 |*Organometallics* 2011, 30, 3284–3292

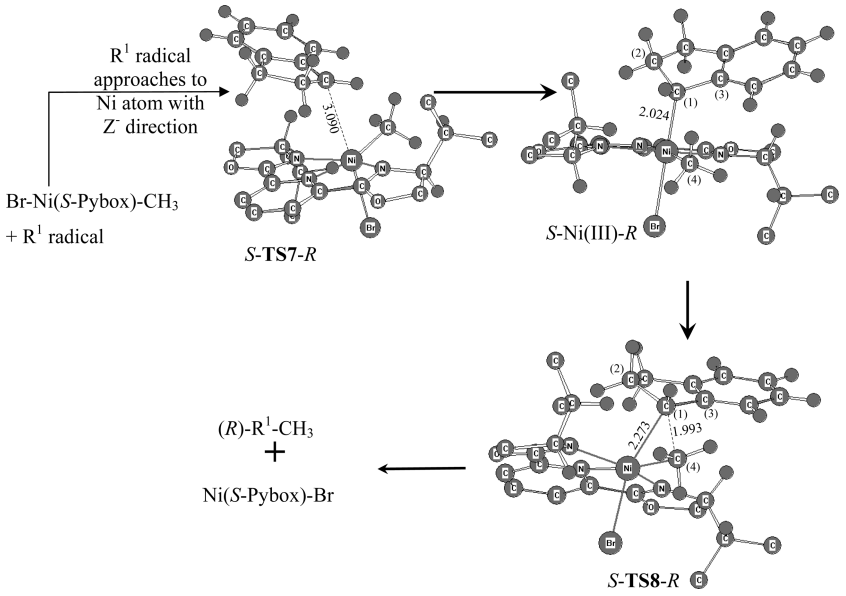

Figure 10. Optimized geometries for the intermediates, the transition states, and the products in the reaction that forms cross-coupled product in *R*-enantiomer form with the ligand *S*-Pybox.

This implies that radical attack in the Z^- direction may take place more easily than that in the Z^+ direction.

The Ni(III) species process that proceeds through the transition states *S*-**TS7**-*S* is denoted as *S*-Ni(III)-*S* (Figure 9), where the Ni−$C^{(1)}$ bond length is 2.033 Å and the $C^{(1)}$ atom is in the *S*-conformation. The Ni(III) species that proceeds via *S*-**TS7**-*R* is denoted as *S*-Ni(III)-*R* (Figure 10), where the Ni−$C^{(1)}$ bond length is 2.024 Å and the $C^{(1)}$ atom is in the *R*-conformation. The reductive elimination of *S*-Ni(III)-*S* affords the coupled product (*S*)-R^1-CH_3 with a transition state *S*-**TS8**-*S*, in which the Ni···$C^{(1)}$ and $C^{(1)}$···$C^{(4)}$ distances are 2.055 and 2.042 Å, respectively. The reductive elimination of *S*-Ni(III)-*R* affords the coupled product (*R*)-R^1-CH_3, with a transition state, *S*-**TS8**-*R*, in which the Ni···$C^{(1)}$ and $C^{(1)}$···$C^{(4)}$ distances are 2.273 and 1.993 Å, respectively. This geometrical information indicates that *S*-**TS8**-*R* occurs later than *S*-**TS8**-*S* along the reaction coordinate in terms of $C^{(1)}$−$C^{(4)}$ bond formation and Ni−$C^{(1)}$ and Ni−$C^{(4)}$ bond cleavages. This implies that the reductive elimination of *S*-Ni(III)-*S* may occur more easily than that of *S*-Ni(III)-*R*.

The free energy profiles shown in Figure 11 support the two hypotheses in the above two paragraphs. Compared to the free energy profile for the case of the Pybox ligand (shown with a dotted line), the use of *S*-Pybox leads to a mild modification of this profile. The radical attack step in the Z^+ direction has a free energy of activation of 16.5 kcal/mol, while that in the Z^- direction has a free energy of activation of 8.9 kcal/mol. The *S*-Ni(III)-*R* species is kinetically more easily formed than *S*-Ni(III)-*S*. *S*-Ni(III)-*R* is a bit more stable than *S*-Ni(III)-*S*, by about 2.8 kcal/mol. However, situation changes in the reductive elimination step (eq *S*-8-*S* or -*R*). The free energy of activation in eq *S*-8-*S* for (*S*)-R^1-CH_3 formation is 17.7 kcal/mol, and that in eq *S*-8-*R* for (*R*)-R^1-CH_3 formation is 27.5 kcal/mol.

(b) Enantioselectivity of the Cross-Coupled Product for Reaction B. As described in part (b) in subsection B, for the Ni(I)−Ni(III) catalytic cycle, the TOF-determining intermediate is the reactant complex from Ni(pybox)-Br and CH_3ZnBr (**RC5**), and the TOF-determining transition state is the transition state of the reductive elimination step (**TS8**-*S*/*R*). When

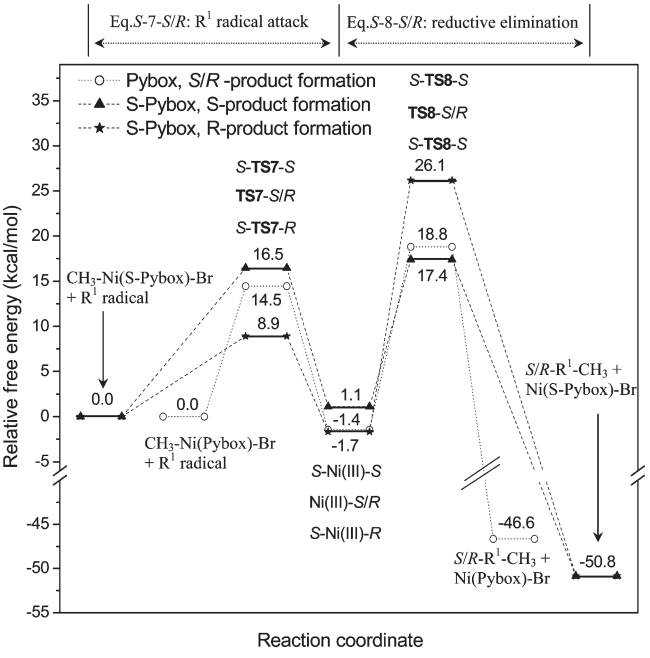

Figure 11. Free energy profiles of eqs *S*-7-*S*/*R* and *S*-8-*S*/*R* for formation of cross-coupled product R^1-CH_3 as both *S* (solid triangles with dashed line) and *R* (solid stars with dashed line) enantiomers. Here *S*-Pybox is used as the ligand of the Ni(I) catalyst. The free energy profile of eqs 7 and 8 where Pybox is used as the ligand (open circles with dotted line) is shown for comparison.

S-Pybox is used as the ligand, the pathways that lead to the *R*-enantiomer and *S*-enantiomer share the same TDI, but have different TDTSs. The difference in the energetic spans for these two pathways is determined by the difference of the free energies for *S*-**TS8**-*R* and *S*-**TS8**-*S*, as can be written as

$$\delta E_R - \delta E_S = G_{S\text{-TS-8}R} - G_{S\text{-TS-8}S} \quad \text{(I)}$$

dx.doi.org/10.1021/om1012049 |*Organometallics* 2011, 30, 3284–3292

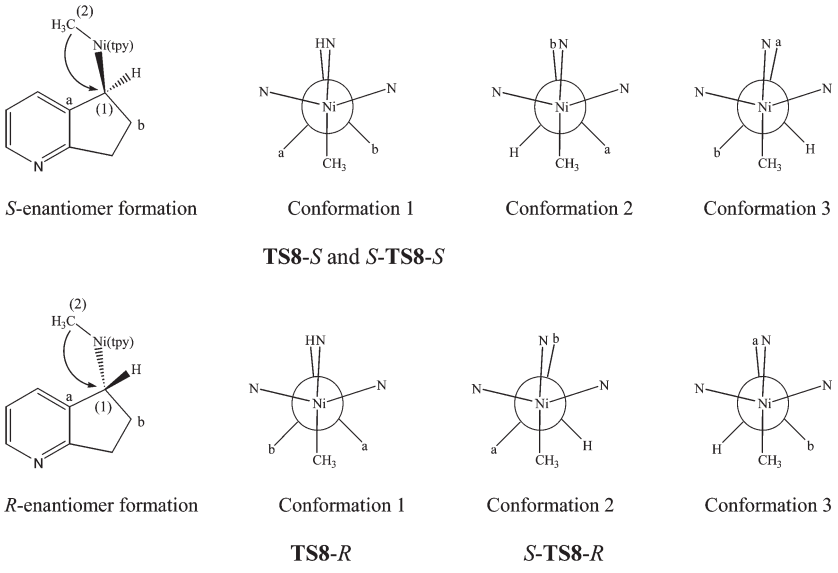

Figure 12. Conformations of the Ni−$C^{(1)}$ bond in the three kinds of possible first-order saddle points when exploring the transition-state structure of the reductive elimination step (eq 8). The round cycle represents the $C^{(1)}$ atom. See text for a detailed description.

Possible side reactions of the R^1 radical were not considered here, because they may not influence the overall enantioselectivity of the coupled product. Therefore, the *S*/*R* ratio can be calculated from the Boltzmann distribution of each transition state[20] for the reductive elimination step (i.e., $G_{S\text{-TS-}8S}$ and $G_{S\text{-TS-}8R}$) at the temperature of 273 K, as the following:

$$[S]/[R] = r_S/r_R = \exp\left[\frac{G_{S\text{-TS-}8R} - G_{S\text{-TS-}8S}}{RT}\right] \qquad \text{(II)}$$

The enantiomeric excess is

$$\text{ee} = \frac{[S]/[R] - 1}{[S]/[R] + 1} \qquad \text{(III)}$$

in the case where the *S*-enantiomer is dominant over the *R*-enantiomer. Using the data in Figure 11 one can easily obtain that the r_S/r_R is 8.9×10^6 with the gas phase model and 4.3×10^6 with consideration of the bulk solvation effect (see Computational Method), which corresponds to an ee value of more than 99%. Although qualitatively this result is consistent with the experimentally measured value (92%),[4a] there is an overestimation somehow. As it has been demonstrated that the ee value changes from 0 to close to 1 when the C_{2v} ligand is replaced with the C_2 ligand, it is reasonable to anticipate that the incorporation of solvent molecules may be disadvantageous to some degree to the asymmetry of the ligand, therefore lowering the calculated ee value. However, presently the solvation effect is considered only by the single-point PCM calculation of the geometries optimized in the gas-phase calculation. We believe the prediction could be more accurate if the geometry optimizations are performed with the PCM calculation.

(c) Discussion of Steric Effect of the S-Pybox Ligand for the Reductive Elimination Step. It has been demonstrated that the reductive elimination step is irreversible and rate-determining. The enantioselectivity of the coupled product may be accounted for by the free energy difference of the transition states of the reductive elimination steps leading to the *S*-enantiomer and *R*-enantiomer products. It may be helpful to carry out conformational analysis for the transition-state structures of the reductive elimination steps in producing both *S*- and *R*-enantiomers, with both the Pybox and *S*-Pybox ligands.

From inspection of the transition-state structures of the reductive elimination step with the Pybox ligand (eq 8), **TS8**-*S* (see Figure 4) and **TS8**-*R*, it was found that the Ni···$C^{(1)}$ bond adopts the conformation as indicated in conformation 1 in Figure 12, where the Ni−$C^{(2)}H_3$ bond lies between the $C^{(1)}$−$C^{(a)}$ and $C^{(1)}$−$C^{(b)}$ bonds. Actually when exploring the PES, another two first-order saddle points, which also have imaginary vibrations of the $C^{(1)}\cdots C^{(2)}$ bond formation/cleavage, were also found. In these two first-order saddle points the Ni···$C^{(1)}$ bond adopts the conformation as indicated in conformations 2 and 3 in Figure 12. The Ni−$C^{(2)}H_3$ bond is between the $C^{(1)}$−H and $C^{(1)}$−$C^{(a)}$ bonds and between the $C^{(1)}$−H and $C^{(1)}$−$C^{(b)}$ bonds. These two kinds of first-order saddle points have higher energies/free energies than those of **TS8**-*S* or **TS8**-*R*.

Because the indene substrate also has a bulky benzene ring, the Ni−$C^{(1)}$ bond could not adopt the three conformations freely when the isopropyl groups are present on the *S*-Pybox ligand. *S*-**TS8**-*S* can still adopt conformation 1, while *S*-**TS8**-*R* cannot adopt conformation 1 because there is a strong steric hindrance between the benzene ring and the isopropyl group. So *S*-**TS8**-*R* has to adopt conformation 2 to lower the steric hindrance, and this may lead to a higher energy/free energy of *S*-**TS8**-*R* than that of *S*-**TS8**-*S* ($G_{S\text{-TS8-R}} > G_{S\text{-TS8-S}}$), which results in the enantioselectivity of the coupled product.

CONCLUSION

(1) By calculation of the energetic spans for both the Ni(0)−Ni(II) mechanism, which contains sequential steps of oxidative addition, transmetalation, and reductive elimination, and the Ni(I)−Ni(III) mechanism, which contains sequential steps of transmetalation, oxidative addition, and reductive elimination, the latter mechanism was found more favorable than the former one.

(2) The enantioselectivity of the coupled product is determined by the difference between the free energies of the transition states of the reductive elimination steps for

dx.doi.org/10.1021/om1012049 |*Organometallics* 2011, 30, 3284–3292

model reaction B. The free energy of activation for the reductive elimination of the *S*-Ni(III)-*R* species in generating the coupled product as the *R*-enantiomer is higher than that of the *S*-Ni(III)-*S* species in generating the *S*-enantiomer, which may account for the high enantioselectivity of reaction B. The method for calculating/predicting the enantioselectivity of the coupled product may help synthetic chemists design/select their catalyst ligands and reactant substrates.

(3) The conversion of racemic alkyl electrophiles to highly enantioselective coupled product is due to the presence of asymmetric steric hindrance of alkyl groups in the *S*-Pybox ligand, which makes the transition state of the reductive elimination step that proceeds to the *S*-enantiomer different from that which proceeds to the *R*-enantiomer.

■ ASSOCIATED CONTENT

Supporting Information. Tables containing atomic coordinates, calculated energies without and with zero-point energy correction (in au), and free energies (in au, at 313.15 K) for all of the stationary structures reported in this paper. This material is available free of charge via the Internet at http://pubs.acs.org.

■ AUTHOR INFORMATION

Corresponding Author
*E-mail: hatrick2009@upc.edu.cn. Fax: +86-532-86981565.

■ ACKNOWLEDGMENT

This research has been supported by the National Science Foundation of China (21003159) and grants from China University of Petroleum (Y0904044, Y0904045). X.F.L. thanks The University of Hong Kong for the computational resources provided.

■ REFERENCES

(1) Books, for example: (a) Diederich, F., Stang, P. J. *Metal-Catalyzed Cross-Coupling Reactions*; Wiley-VCH: Weinheim, Germany; 1998. (b) de Meijere, A.; Diederich, F. *Metal-Catalyzed Cross-Coupling Reactions*, 2nd ed.; Wiley-VCH: Weinheim, Germany; 2004. (c) Beller, M.; Bolm, C. *Transition Metals for Organic Synthesis*, 2nd ed.; Wiley-VCH: Weinheim, 2004.

(2) For reviews: (a) Cárdenas, D. J. *Angew. Chem., Int. Ed.* **1999**, *38*, 3018–3020. (b) Luh, T. Y.; Leung, M. K.; Wong, K. T. *Chem. Rev.* **2000**, *100*, 3187–3204. (c) Cárdenas, D. J. *Angew. Chem., Int. Ed.* **2003**, *42*, 384–387. (d) Frisch, A. C.; Beller, M. *Angew. Chem., Int. Ed.* **2005**, *44*, 674–688. (e) Phapale, V. B.; Cárdenas, D. J. *Chem. Soc. Rev.* **2009**, *38*, 1598–1607.

(3) (a) Zhou, J.; Fu, G. C. *J. Am. Chem. Soc.* **2003**, *125*, 14726–14727. (b) Powell, D. A.; Fu, G. C. *J. Am. Chem. Soc.* **2004**, *126*, 7788–7789. (c) Zhou, J.; Fu, G. C. *J. Am. Chem. Soc.* **2004**, *126*, 1340–1341.

(4) For asymmetric cross-coupling: (a) Arp, F. O.; Fu, G. C. *J. Am. Chem. Soc.* **2005**, *127*, 10482–10483. (b) Fischer, C.; Fu, G. C. *J. Am. Chem. Soc.* **2005**, *127*, 4594–4595. (c) González-Bobes, F.; Fu, G. C. *J. Am. Chem. Soc.* **2006**, *128*, 5360–5361. (d) Smith, S. W.; Fu, G. C. *Angew. Chem., Int. Ed.* **2008**, *47*, 9334–9336.

(5) For cross-coupling of secondary C(sp^3) electrophiles with C(sp^2) neucleophiles: (a) Smith, S. W.; Fu, G. C. *J. Am. Chem. Soc.* **2008**, *130*, 12645–12647. (b) Lou, S.; Fu, G. C. *J. Am. Chem. Soc.* **2010**, *132*, 5010–5011.(c) Lunding, P. M.; Fu, G. C. *J. Am. Chem. Soc.* **2010**, *132*, 11027−11029.

(6) (a) Terao, J.; Watanabe, H.; Ikumi, A.; Kuniyasu, H.; Kambe, N. *J. Am. Chem. Soc.* **2002**, *124*, 4222–4223. (b) Terao, J.; Todo, H.; Watanabe, H.; Ikumi, A.; Kambe, N. *Angew. Chem., Int. Ed.* **2004**, *43*, 6180–6182.

(7) (a) Hadei, N.; Kantchev, E. A. B.; O'Brien, C. J.; Organ, M. G. *Org. Lett.* **2005**, *7*, 3805–3807. (b) Hadei, N.; Kantchev, E. A. B.; O'Brien, C. J.; Organ, M. G. *J. Org. Chem.* **2005**, *70*, 8503–8507.

(8) Jones, G. D.; Martin, J. L.; McFarland, C.; Allen, O. R.; Hall, R. E.; Haley, A. D.; Brandon, R. J.; Konovalova, T.; Desrochers, P. J.; Pulay, P.; Vicic, D. A. *J. Am. Chem. Soc.* **2006**, *128*, 13175–13183.

(9) Lin, X.; Phillips, D. L. *J. Org. Chem.* **2008**, *73*, 3680–3688.

(10) (a) Phapale, V. B.; Buñuel, E.; García-Iglesias, M.; Cárdenas, D. J. *Angew. Chem., Int. Ed.* **2007**, *46*, 8790–8795. (b) Phapale, V. B.; Guisán-Ceinos, M.; Buñuel, E.; Cárdenas, D. J. *Chem.—Eur. J.* **2009**, *15*, 12681–12688.

(11) One step of oxidative addition and reductive elimination reported: Wang, M.; Lin, Z. *Organometallics* **2010**, *29*, 3077–3084.

(12) (a) Becke, A. D. *Phys. Rev. A* **1988**, *38*, 3098–3100. (b) Lee, C.; Yang, W.; Parr, R. G. *Phys. Rev. B* **1988**, *37*, 785–789. (c) Becke, A. D. *J. Chem. Phys.* **1993**, *98*, 5648–5653.

(13) Frisch, M. J.; Trucks, G. W.; Schlegel, H. B.; Scuseria, G. E.; Robb, M. A.; Cheeseman, J. R.; Montgomery, J. A., Jr.; Vreven, T.; Kudin, K. N.; Burant, J. C.; Millam, J. M.; Iyengar, S. S.; Tomasi, J.; Barone, V.; Mennucci, B.; Cossi, M.; Scalmani, G.; Rega, N.; Petersson, G. A.; Nakatsuji, H.; Hada, M.; Ehara, M.; Toyota, K.; Fukuda, R.; Hasegawa, J.; Ishida, M.; Nakajima, T.; Honda, Y.; Kitao, O.; Nakai, H.; Klene, M.; Li, X.; Knox, J. E.; Hratchian, H. P.; Cross, J. B.; Adamo, C.; Jaramillo, J.; Gomperts, R.; Stratmann, R. E.; Yazyev, O.; Austin, A. J.; Cammi, R.; Pomelli, C.; Ochterski, J. W.; Ayala, P. Y.; Morokuma, K.; Voth, G. A.; Salvador, P.; Dannenberg, J. J.; Zakrzewski, V. G.; Dapprich, S.; Daniels, A. D.; Strain, M. C.; Farkas, O.; Malick, D. K.; Rabuck, A. D.; Raghavachari, K.; Foresman, J. B.; Ortiz, J. V.; Cui, Q.; Baboul, A. G.; Clifford, S.; Cioslowski, J.; Stefanov, B. B.; Liu, G.; Liashenko, A.; Piskorz, P.; Komaromi, I.; Martin, R. L.; Fox, D. J.; Keith, T.; Al-Laham, M. A.; Peng, C. Y.; Nanayakkara, A.; Challacombe, M.; Gill, P. M. W.; Johnson, B.; Chen, W.; Wong, M. W.; Gonzalez, C.; Pople, J. A. *Gaussian 03*, Revision C.02; Gaussian, Inc.: Wallingford, CT, 2004.

(14) (a) Miertus, S.; Scrocco, E.; Tomasi, J. *Chem. Phys.* **1981**, *55*, 117–129. (b) Miertus, S.; Tomasi, J. *Chem. Phys.* **1982**, *65*, 239–245. (c) Cossi, M.; Barone, V.; Cammi, R.; Tomasi, J. *Chem. Phys. Lett.* **1996**, *255*, 327–335. (d) Cossi, M.; Scalmani, G.; Rega, N.; Barone, V. *J. Chem. Phys.* **2002**, *117*, 43–54.

(15) As the solvent of DMA is not available in Gassuain 03, DMSO (dielectric constant $\varepsilon = 47$) was used to model DMA ($\varepsilon = 38$).

(16) (a) Gonzalez, C.; Schlegel, H. B. *J. Chem. Phys.* **1989**, *90*, 2154–2161. (b) Gonzalez, C.; Schlegel, H. B. *J. Phys. Chem.* **1990**, *94*, 5523–5527.

(17) (a) Kozuch, S.; Amatore, C.; Jutand, A.; Shaik, S. *Organometallics* **2005**, *24*, 2319–2330. (b) Kozuch, S.; Shaik, S. *J. Am. Chem. Soc.* **2006**, *128*, 3355–3365. (c) Kozuch, S.; Shaik, S. *Acc. Chem. Res.* **2011**, *44*, 101–110.

(18) Kochi, J. K. *Pure Appl. Chem.* **1980**, *52*, 571–605.

(19) Klein, A.; Budnikova, Y. H.; Sinyashin, O. G. *J. Organomet. Chem.* **2007**, *692*, 3156–3166.

(20) Balcells, D; Maseras, F. *New J. Chem.* **2007**, *31*, 334–343.